

# Adiabatic and Intrinsic Modes for Wave Propagation in Guiding Environments with Longitudinal and Transverse Variation: Continuously Refracting Media

Leopold B. Felsen, *Life Fellow, IEEE*, and Levent Sevgi

**Abstract**—The adiabatic and intrinsic mode formalism for nonuniform propagation environments, developed and tested in a companion paper, is now applied to continuously refracting media. The first example involves a guiding refractive index profile with transverse and longitudinal, but coordinate separable, variation that may be regarded as a prototype for this class of waveguides. The second example involves a nonseparable profile with a guiding-to-antiguinding transition that converts an initially well trapped mode into a radiated beam. Both examples demonstrate the problems encountered in achieving a good parametrization for tracking mode-like wave phenomena under rather general conditions.

## I. INTRODUCTION

IN the companion paper [1], we have tested the intrinsic mode (IM) formalism for propagation in longitudinally varying guiding environments on a canonical wedge configuration, which has simple exact solutions in an "appropriate" separable coordinate system. From this canonical test for guiding between physical boundaries, it has been learned how to reparametrize the IM problem from the initially given description in the global rectilinear  $(x, z)$  coordinate frame to "better adapted" local curvilinear  $(u, v)$  coordinates. It has been found that in *weakly* varying guiding regions, away from cutoff transitions due to narrowing waveguide cross section, the IM reduce to the simpler adiabatic modes (AM) but that the IM uniformize the AM through the mode-dependent propagation-to-evanescent cutoff regime where the AM fail. Moreover, in the better adapted  $(u, v)$  coordinates, the IM has reproduced the uniform asymptotic canonical (exact) solution, without the constraint of *weak* longitudinal dependence. This suggests that the spectral content of the IM is adequate for treating regular and cutoff transition phenomena

even under noncanonical conditions because the basic IM formulation does not rely on exact separability.

In the present paper, the IM is applied to continuously refracting environments with transverse and longitudinal variations in the index profile, first for a trapping canonical separable case (Section II) and then for a guiding-to-antiguinding noncanonical case (Section III). For the former, the "properly parametrized" IM again produces the correct uniform asymptotic solution without the constraint to weak longitudinal dependence. In both cases it is confirmed, as anticipated, that cutoff transitions cause no difficulties. However, in the  $(x, z)$  description, the IM fails in guiding-to-antiguinding transitions, in which an initially trapped mode is transformed into a radiated beam. By invoking analytic continuation of the  $(x, z)$  parametrized IM spectra from the strongly guiding side, where they are valid, to the strongly antiguiding side (avoiding the transitional domain), one finds that the resulting  $(x, z)$  parametrized AM and IM properly describe certain features of the field but not directly the detached entire beam-type field in the antiguiding region. On the other hand, it is found that the better adapted  $(u, v)$  parametrization not only improves the IM on the guiding side but naturally develops the detaching beam in the transition region. These observations are supported by preliminary numerical results. Conclusions from the two-part sequence are presented in Section IV.

In the presentation, repeated reference is made to equations, figures, and discussion in [1]. Such references are identified by the prefix (1.) whereas *literature* references at the end of [1] are identified by [1.] in square brackets.

## II. CANONICAL GRADED INDEX WAVEGUIDE

To illustrate the IM formalism for a guiding environment established by refraction, we consider a medium with locally parabolic refractive index  $n(x, z)$  that renders the wave equation nonseparable in the  $(x, z)$  coordinates [2],

$$n^2(x, z) = 1 - \frac{b_0^2 x^2}{(D + z)^4} \quad (1)$$

where  $x$  and  $z$  are transverse and longitudinal coordinates, respectively, and  $b_0$  is a constant having dimension of length. However, in cylindrical  $(\phi, \rho)$  coordinates defined by

Manuscript received June 14, 1990; revised February 25, 1991. This work was supported in part by the Joint Services Electronic Program under Contract F49620-88-C-0075, by the Naval Ocean Systems Center, and by a Fellowship from the Department of Electrical-Electronic Engineering, Technical University of Istanbul, Turkey.

L. B. Felsen is with the Department of Electrical Engineering/Weber Research Institute, Polytechnic University, Farmingdale, NY 11735.

L. Sevgi was with the Department of Electrical Engineering/Weber Research Institute, Polytechnic University, Farmingdale, NY, on leave from the Department of Electrical-Electronic Engineering, Technical University of Istanbul, 80626 Maslak/Istanbul, Turkey.

IEEE Log Number 9100562.

0018-926X/91\$01.00 ©1991 IEEE

$x = \rho \sin \phi$ ,  $z = \rho \cos \phi - D$ , and restricting to small angles, (1) yields the separable profile

$$\hat{n}^2(\phi, \rho) = 1 - \frac{b_0^2 \phi^2}{\rho^2}. \quad (2)$$

In either case, the refractive index decays monotonically (quadratically) away from the guide axis  $x = 0$  or  $\phi = 0$ , with constant refractive index contours shown in Fig. 1. Because  $\hat{n}^2 \rightarrow -\infty$  as  $x \rightarrow \infty$ , there is no energy leakage from this model environment. The wave equation is  $(\phi, \rho)$  separable and yields the exact solutions

$$W_q(\phi, \rho) = F_q(\phi) \{ J_\mu(k_0 \rho) \text{ or } H_\mu^{(1)}(k_0 \rho) \} \quad (3)$$

$$F_q(\phi) = C_0 \exp(-k_0 b_0 \phi^2 / 2) \underline{H}_q \{ (k_0 b_0)^{1/2} \phi \},$$

$$\mu = [k_0 b_0 (2q + 1)]^{1/2} \quad (3a)$$

where  $\underline{H}_q(w)$  is the Hermite polynomial,  $C_0 = (2^q q! \sqrt{\pi})^{-1/2}$  is its normalization coefficient, and  $\mu$  is the modal eigenvalue. Thus, this graded index taper can serve as a canonical test for IM confined by continuous refraction, just as the wedge in Section 1.II-A serves as a test for IM confined by physical boundary reflection. The ray and mode field behavior in this medium have been discussed in detail in [2].

For the IM construction, the first task is the determination of the modal caustics via (1.9). As mentioned earlier [1], this cannot be done as yet in the preferred coordinates  $(u, v)$  because their choice requires a knowledge of the caustic curve. We therefore begin with the  $(x, z)$  parametrization, using (1) for small  $x/z$  to justify the adiabatic approximation; in the  $(x, z)$  version of (1.9), we set  $\beta_q^2 = k_0^2 \hat{n}_0^2(x_{c_q}, z)$  (see (1.9a)) and  $u_1 = -u_2 \rightarrow x_{c_q}$ . On the left-hand side of (1.9), in the second term, the reflection coefficients are replaced by the values appropriate to caustics  $\Gamma_{1,2} = \exp(-i\pi/2)$ . Direct integration of (1.9), modified as noted and using (1), yields

$$x_{c_q}(z) = \pm d_0^{1/2} (D + z),$$

$$d_0 = \frac{(2q + 1)}{k_0 b_0}, \quad x/z \ll 1. \quad (4)$$

Thus, subject to these approximations, the caustics are straight lines emanating from the point  $z = -D$  on the negative  $z$ -axis with angles  $\pm \phi_{c_q}$  (see Fig. 1; as in [1], dimensions of lengths in various plots are in arbitrary units, which are not indicated explicitly). As a logical first try, the local orthogonal coordinates  $(u, v)$  are chosen to be cylindrical polar with  $u = \phi \leq \phi_{c_q}$ ,  $\rho = [(z + D)^2 + x^2]^{1/2}$ , where  $\phi_{c_q}$  is restricted to be small. While this choice turns out to be optimal because the problem is strictly  $(\phi, \rho)$  separable, a procedure like that in [1.18] should be pursued for more general nonseparable conditions.

We now construct the IM in (1.6) in the preferred coordinates  $(\phi, \rho)$ , in which relevant quantities are identified by a caret. From (4),  $\phi_{c_q}^\pm = \pm d_0^{1/2}$ . It is found that  $\hat{\beta}_q(\hat{\rho})$ ,  $\hat{\rho}_q(\hat{\beta})$ ,  $\hat{a}_q(\hat{\beta})$ , and  $\hat{\Omega}_q(\hat{\beta})$  are exactly the same as for the wedge problem in [1] (see text between (1.12) and (1.13)) provided

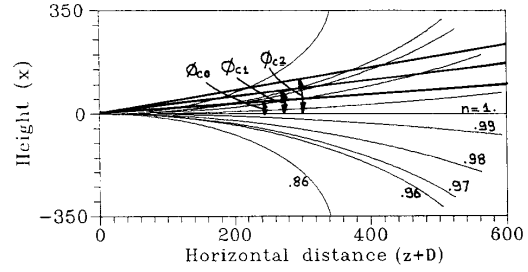


Fig. 1. Constant refractive index contours for trapping refractive index profile in (2). Also shown are the upper caustics at the angles  $\phi_{c_q} \approx 10, 17, 23^\circ$  for modes  $q = 0, 1, 2$ ;  $b_0 = 3.32 \cdot 10^2$ .

that the eigenvalue  $\mu$  is the one specified in (3a). The adiabatic transverse wave function  $\hat{U}_q$  satisfies the locally adapted equation in the  $\phi$ -domain [see (1.7a), with  $u = \phi$ ,  $v = \rho$ ,  $h_\phi = \rho$ ,  $h_\rho = 1$ ] which, with  $\hat{k}^2(\phi, \rho) = k_0^2 \hat{n}^2(\phi, \rho)$  taken from (2), establishes these mode functions as  $\hat{U}_q(\phi, \rho) = \rho^{-1/2} F_q(\phi)$  in (3a). It then follows that the IM spectral integral is the same as in (1.14) provided that  $\hat{U}_q$  from (1.13) is replaced by  $\hat{U}_q$  here. As noted in the discussion of (1.14), the asymptotic (AM) approximation of the integral yields the asymptotic form of the Bessel function in (3), which fails in the cutoff region  $\rho \rightarrow \mu$ . The IM is uniform through cutoff. Because  $\hat{U}_q$  is exact (see Fig. 2 for typical mode shapes), the AM and IM forms in the well-adapted  $(u, v)$  coordinates in this example are not constrained to the initially assumed weak longitudinal dependence (small  $\phi_{c_q}$ ). This is not true in the original  $(x, z)$  system where the AM and IM behavior is directly analogous to the one summarized in the last paragraph of Section 1.III.

### III. LONGITUDINALLY DEPENDENT LINEAR PROFILE: GUIDING-TO-ANTIGUIDING

A simple nonseparable, yet nontrivial, refractive index variation that continuously covers the range from cutoff and strong trapping to antiguiding through a guiding-to-antiguiding transition is expressed by the longitudinally and transversely linear profile

$$k^2(x, z) = k_0^2 [1 + (a_0 z) x],$$

$$a_0 > 0, \quad x > 0, \quad -\infty < z < +\infty \quad (5)$$

which is bounded at  $x = 0$  by a perfectly conducting plane. Here  $(a_0 z)$  is regarded as the  $z$ -dependent slope of the transverse  $(x)$  profile, with  $a_0$  (dimension of length<sup>-2</sup>) small enough to ensure gradual change (see Fig. 3 for constant refractive index contours). The profile in (5) has been chosen because it has been treated previously in a similar context (see [1.12]). For  $z < 0$ , the profile defines a guiding region (surface duct) between the boundary and the modal caustic  $x_{c_q}(z)$  corresponding to mode  $q$  (Fig. 3). Because  $k(x, z) \rightarrow \infty$  as  $x \rightarrow \infty$ , then as in the analogous canonical problem in Section II, trapping is complete, i.e., there is no leakage. Advancing along the negative  $z$ -direction, the duct narrows and eventually causes cutoff of mode  $q$  at  $z = z_{tq}$  where the local longitudinal wavenumber  $\beta_q(z) = 0$ . The cutoff transition is described uniformly by the IM spectral

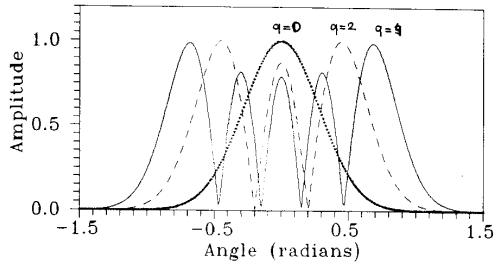


Fig. 2. Transverse profiles  $\hat{U}_q$  (Gaussian Hermite functions) for the first three even numbered modes  $q = 0, 2, 4$  in the graded index waveguide specified in (2), with  $b_0 = 3.32 \cdot 10^2$ ,  $k_0 = 0.105$  rad/m.

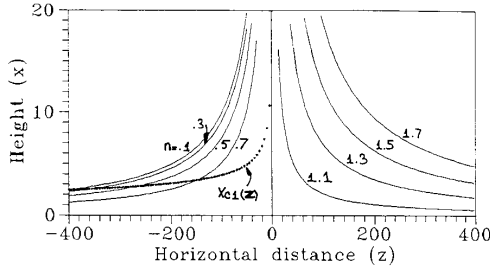


Fig. 3. Constant refractive index contours for guiding-to-antiguating refractive index profile in (5) with  $a_0 = 10^{-4}$ . Also shown is the caustic for the lowest order mode  $q = 1$ . Cutoff for this mode occurs at  $z_c \approx -4070$ .

integral just as in Section II. Advancing along the positive  $z$ -direction on the guiding side, the duct cross section widens until the duct disappears at  $z = 0$ . For  $z > 0$ , the profile is antiguiding and refracts waves away from the boundary.

We shall treat magnetically polarized waves for which the IM wavefunction  $W_q(x, z)$  in (1.1) satisfies the boundary condition

$$\left. \frac{d}{dx} W_q(x, z) \right|_{x=0} = 0. \quad (6)$$

Then in the guiding region  $z < 0$ , referring to the IM spectral integral in (1.6), the quantities in the integrand, as specified in (1.6a)-(1.6c), are given as follows for the profile in (5):

$$\bar{z}_q(\beta) = \frac{1}{B_0} \tau^{3/2}, \quad \tau = k_0^2 - \beta^2, \quad B_0 = a_0 k_0^2 \sigma_q^{3/2} \quad (7a)$$

$$a_q(\beta) = \left[ \frac{-3}{B_0} \tau^{1/2} \right]^{1/2} \quad (7b)$$

$$\Omega_q(\beta) = \frac{-3}{B_0} \left\{ \frac{-\beta}{4} \tau^{3/2} + \frac{k_0^2 \beta}{8} \tau^{1/2} + \frac{k_0^4}{8} \sin^{-1} \left( \frac{\beta}{k_0} \right) \right\} \quad (7c)$$

$$U_q(x, \bar{z}(\beta), \beta) = C_0 \text{Ai}(\xi),$$

$$C_0 = \sigma_q^{1/4} \frac{1}{\tau^{1/4} \text{Ai}(-\sigma_q)} \quad (7d)$$

$$\xi = -\sigma_q \left\{ 1 - \frac{x}{x_{cq}} \right\}. \quad (7e)$$

Here,  $\text{Ai}(\sigma)$  is the Airy function [1.12], and  $\sigma_q$  is the root of  $\text{Ai}'(-\sigma_q) = 0$ , with the prime denoting the derivative with respect to the argument. The transverse adiabatic mode function  $U_q$  satisfies the local equation (1.3), which has the normalized solution shown in (7d). From (1.9) and (1.9a), the modal caustic, which parametrizes the solution, is found to be located at

$$x_{cq}(z) = -\sigma_q (a_0 k_0^2 z)^{-1/3},$$

$$-z = |z| \exp(i3\pi), \quad (8)$$

with  $z$  defined as shown to ensure that  $x_{cq}(z) > 0$  for  $z < 0$ . It then follows from (1.9a) that

$$\beta_{(q)}(z) = \pm \left[ k_0^2 - \sigma_q (a_0 k_0^2 z)^{2/3} \right]^{1/2} \quad (9)$$

which yields by inversion  $\bar{z}_q(\beta)$  in (7a). These relations are substituted into the spectral integrand in (1.6).

The longitudinal wavenumber  $\beta_{(q)}(z)$  in (9) over its propagating (real  $\beta$ ) range behaves typically as plotted in Fig. 4. Cutoff of the  $q$ th AM occurs at  $z = z_{1q}$  where  $\beta_{(q)}(z_{1q}) = 0$ ; for  $|z| > |z_{1q}|$ , with  $\beta_{(q)} = i|\beta_{(q)}|$ , the fields are evanescent. As  $z \rightarrow 0$ , one has  $\beta_{(q)} \rightarrow \pm k_0$ , i.e., the wave spectra are entirely longitudinal (along  $z$ ). Simultaneously, the caustic recedes to  $x \rightarrow \infty$  (see (8) and Fig. 3), thereby making the duct cross section unbounded and signaling the failure of the  $(x, z)$  parametrized adiabatic mode spectra there. However, as will be seen, this failure can be removed by passing to better adapted curvilinear  $(u, v)$  coordinates (see Section 1.IIB).

On the antiguiding side  $z > 0$ , the AM and therefore the IM problem in the  $(x, z)$  parametrization is undefined. However, we may inquire as to what happens when, by analytic continuation, the IM spectral integral is extended *formally* to the antiguiding region. Far enough away from the transition region, the analytically extended caustic parameter  $x_{cq}(z)$  in (8), with  $z \rightarrow -z$ , remains bounded but is complex. The resulting adiabatic mode, which must satisfy an outgoing wave condition at  $x \rightarrow \infty$ , is *leaky* and *grows* toward  $x \rightarrow \infty$ . The "AM" still satisfies (1.3), with (5) and the boundary condition in (6) at  $x = 0$ . Implementing these steps yields

$$\tilde{U}_q(x, \bar{z}(\beta); \beta) = -\frac{1}{2} \exp(-i2\pi/3) \cdot W_1 \left[ \alpha_q - x / (a_0 k_0^2 |z|)^{-1/3} \right] \quad (10)$$

$$W_1(\xi) \equiv -2 \exp(i2\pi/3) \text{Ai}(\xi \exp(i2\pi/3)) \quad (11a)$$

with  $\alpha_q = -\sigma_q \exp(-i2\pi/3)$ , where  $\alpha_q$  is the root of  $W_1(-\alpha_q) = 0$ . The complex caustic location is

$$\bar{x}_{cq}(z) = -\sigma_q (a_0 k_0^2 |z| \exp(i2\pi))^{-1/3} = x_{cq}(z) \exp(-i5\pi/3) \quad (11b)$$

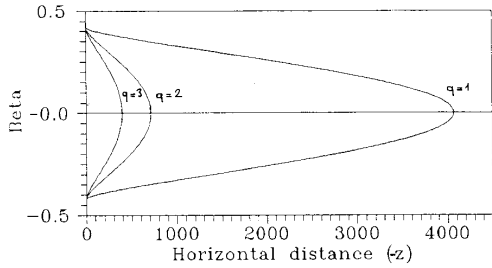


Fig. 4. Variation of the longitudinal spectral wavenumber  $\beta$  for the profile in Fig. 3 between the cutoff point  $z_{iq}$  (where  $\beta = 0$ ) and the guiding-to-antiguiding transition point  $z = 0$ . Modes  $q = 1, 2, 3$ .  $k_0 = 4\pi$  rad/m.

and the definition of  $z = |z| \exp(i2\pi)$  for  $z > 0$  is consistent with that in (8) for  $z < 0$ . The  $\tilde{\beta}_{(q)}$  corresponding to  $\beta_{(q)}$  in (9) becomes

$$\tilde{\beta}_{(q)}(z) = \left[ k_0^2 - \sigma_q (a_0 k_0^2 |z|)^{2/3} \exp(i4\pi/3) \right]^{1/2}. \quad (12)$$

Constructing the IM integral and performing its asymptotic evaluation at the saddle points  $\beta_{(qs)} = \beta_q$  and  $\beta_{(qs)} = \tilde{\beta}_q$  corresponding to the integrands in (7)–(9) and in (10) and (11) outside the transition region  $z \cong 0$  on the guiding and antiguiding sides, respectively, one obtains the AM solution

$$\tilde{W}_q(x, z) \approx (2\pi)^{1/2} \frac{\text{Ai}[-\sigma_q(1-x/x_{cq})] \exp[i\Omega_q(\beta_q)]}{(a_0 k_0^2 |z|)^{1/6} (\beta_q)^{1/2} \text{Ai}(-\sigma_q)} \quad (13a)$$

on the guiding side  $z < 0$ , and

$$\tilde{W}_q(x, z) \approx \frac{\sigma_q^{1/4} / 2W_1 \left[ \alpha_q - x / (a_0 k_0^2 |z|)^{-1/3} \right]}{\text{Ai}(-\sigma_q) |\beta_{qs}|^{1/2}} \cdot \exp[i(\Omega_q(\beta_{qs}) + 7\pi/12)] \quad (13b)$$

on the antiguiding side  $z > 0$ . For underwater acoustic propagation, analogous AM solutions were obtained previously in [1.12], and they were compared there with an independent numerical parabolic equation (PE) solution. It was found that the AM and PE, outside the transition region near  $z = 0$ , agree on the guiding side but that the  $(x, z)$  parametrized AM on the antiguiding side predicts only the initial growth of the field away from the boundary at  $x = 0$  without the eventual peaking and decay (i.e., the beam) that is found from PE (see Fig. 5). For the present problem, the  $\tilde{AM}$  behavior in (13b) is shown in Fig. 6. One may only infer indirectly, through the truncation of the leaky wave domain at  $z \approx 0$ , that a beam-type field exists away from the boundary (see Fig. 7).

A “better adapted” parametrization, as discussed in Section 1.IB, should be based on local separability of the wave equation in  $(u, v)$  coordinates that assign to the caustic  $x_{cq}(z)$  and the boundary  $x = 0$  the curvilinear coordinates  $u_2 = u_{cq} = 1$  and  $u_1 = 0$ , respectively. As a first approximation, for the  $v = \text{constant}$  surfaces, we choose local circular contours that intersect the  $u = 1$  and  $u = 0$  boundaries

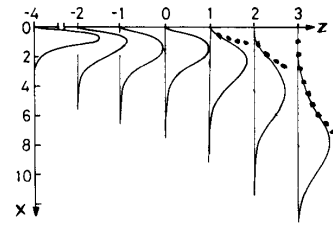


Fig. 5. Adiabatic mode (AM) and parabolic equation (PE) calculation of lowest mode in an underwater acoustic guiding-to-antiguiding transition region modeled as in (5) but with a Dirichlet boundary condition ( $W_q = 0$  at  $x = 0$ ) instead of (6) (see [1.12]). Mode profiles are shown in various  $z = \text{const.}$  cross sections. Solid curves: numerically implemented PE (taken as the reference solution). For  $z \leq -1$  (well-guided regime), AM and PE agree very well (comparison not shown). For  $z \geq 1$  (leaky regime), the monotonically increasing  $\tilde{AM}$  (dots) describes only the initial growth of the detaching beam.  $x$  and  $z$  scales are in arbitrary units. AM and  $\tilde{AM}$  are invalid in the guiding-to-antiguiding transition region  $|z| < 1$ .

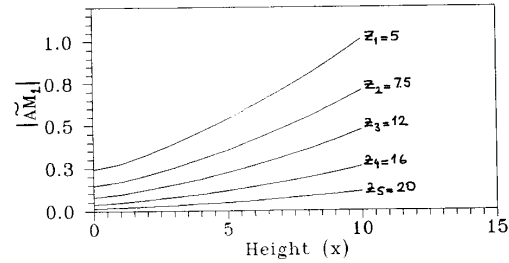


Fig. 6. Initial growth, with height  $x$ , of the analytically continued adiabatic mode  $\tilde{AM}_1$  in (13b) in cross sections  $z = \text{const.}$  Parameters as in Figs. 3 and 4.

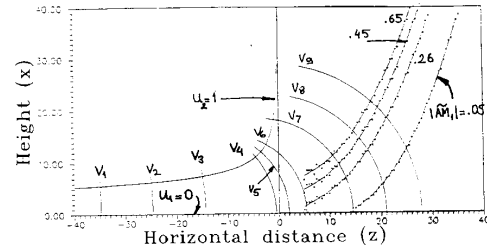


Fig. 7. Constant amplitude contours for mode  $\tilde{AM}_1$  corresponding to the amplitude profiles in Fig. 5. Because the analytically continued AM exist only for  $z > z_0$  (the loosely defined location  $z_0$  is outside the transition region), and because the antiguide leaky modes are launched from the boundary  $x = 0$  only when  $z > 0$ , there exists a limiting upper constant-amplitude contour launched from  $x = 0$  near  $z = 0$ , beyond which the field decreases. Therefore,  $\tilde{AM}_1$  behaves like a beam in  $z = \text{const.}$  cross sections. The limiting value  $|\tilde{AM}_1| = 0.65$  assigned here is merely qualitative and is intended only to show trends. Also shown is the “better adapted”  $(u, v)$  coordinate system which assigns the constant values  $u_1 = 0$  and  $u_2 = 1$  to  $x = 0$  and  $x = x_{c1}(z)$ , respectively. The  $v = \text{const.}$  contours are chosen heuristically as arcs of local circles that intersect  $u_1$  and  $u_2$  orthogonally. Unlike the  $(x, z)$  parametrization, the  $(u, v)$  parametrization retains meaning through the transition region into the antiguiding region.

orthogonally (see Fig. 7). Note that this choice does *not* take into account the effect of the medium variations that have to be included in a more systematic improved procedure for local separability. Although the caustic  $x_{cq}(z)$  and the transverse cross sections  $z = \text{const.}$  in the  $(x, z)$  parametrization exist only on the guiding side  $z < 0$ , the  $v = \text{const.}$  cross

sections in the chosen  $(u, v)$  parametrization extend through the transition region into the antiguiding side. On the circular contours  $v = \text{const.}$ , we determine numerically the refractive index variation  $\hat{k}^2(u, v)$  (see Fig. 8) and can then solve for the cross sectional AM wave functions  $\hat{U}_q(u, v; \hat{\beta}_q(v))$  and eigenvalues  $\hat{\beta}_q(v)$  defined in (1.7a). The eigenvalues can be determined asymptotically from (1.9), with (1.9a), and the wave functions  $\hat{U}_q$  from uniform asymptotics (see (1.10)), allowing smooth transition through isolated turning points  $u_{cq}$  where  $\hat{\beta}_q^2(v) = \hat{k}^2(u_{cq}, v)$ . The  $(u, v)$  parametrized numerical calculation of  $\hat{U}_q$  has been performed on the guiding side, where it improves the  $(x, z)$  parametrized results as in the discussion in Section II (see Fig. 9). Numerical  $(x, z)$  and  $(u, v)$  calculations have also been performed near and through mode cutoff on the guiding side, with results and conclusions similar to those stated in Section I.IV. On the antiguiding side, emphasis so far has been on understanding the *phenomenology* in order to be able to develop systematic parameterization of the mode-beam conversion. As the following discussion shows, this understanding has been achieved, with the use throughout of only modest computer facilities (IBM AT-80286, with 12 MHz speed).

One observes from Fig. 8 that as  $v$  progresses, the medium properties expressed by  $\hat{k}^2(u, v)$  on  $v$ -const. cross sections change from being quasilinearly monotonic on the guiding side to passing through a beam forming maximum on the antiguiding side. The former profiles admit of a single turning point  $u_{cq}^{(1)}$  that defines the original caustic curve  $u_{cq}^{(1)}(v)$  whereas the latter profiles may also admit a second turning point  $u_{cq}^{(2)}$  which defines another caustic  $u_{cq}^{(2)}(v)$ . Thus, the AM field which is confined between the caustic and the boundary in the guiding region, becomes gradually detached from the boundary so as to develop in the antiguiding region a beam that is confined eventually between two caustics.

This behavior can be confirmed by modal ray tracing from the guiding to the antiguiding side. The well-trapped AM in  $z < 0$  is synthesized by two local plane waves (and their corresponding ray congruences) propagating toward the boundary and toward the caustic, respectively. Following the modal rays, one observes their gradual transformation into a single progressing beam on the  $z > 0$  side (see Fig. 10). Numerical modal ray tracing is, in fact, expected to be a very effective procedure for choosing a good  $(u, v)$  parametrization because it *identifies* the caustics *properly*. The scheme chosen so far (circular  $v$ -const. contours) is *ad hoc* and for qualitative illustration only. It does not guarantee the local separability implied in the determination of the AM via the  $(u, v)$  versions of (1.3) and (1.4), although the AM in the  $(u, v)$  parametrization certainly are much better adapted to the physical behavior of the wavefield than in the  $(x, z)$  parametrization. The systematic modal ray tracing routine would specify the caustics numerically, and this data is then incorporated into the numerical IM and AM algorithm. This refined procedure is under investigation.

IV. SUMMARY

In this two-part sequence of papers, we have sought to extend the concept of adiabatic and intrinsic modes to wave

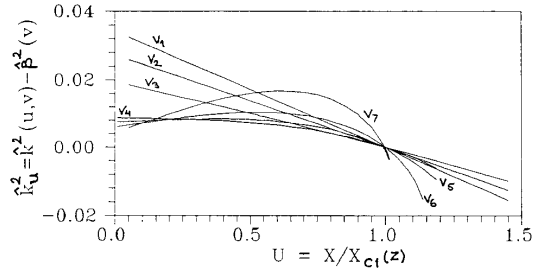


Fig. 8. Variation of normalized refractive index profile  $[\hat{k}^2(u, v) - \hat{\beta}^2(v)]$  along  $v = \text{const.}$  cross sections in Fig. 7 with  $\hat{\beta}^2(v) = \hat{k}^2(u_1, v)$ . Note that the profile changes from being monotonic (quasi-linear) on the guiding side to having a central maximum on the antiguiding side. This latter profile produces a surface-detached beam by refractive confinement around the maximum.

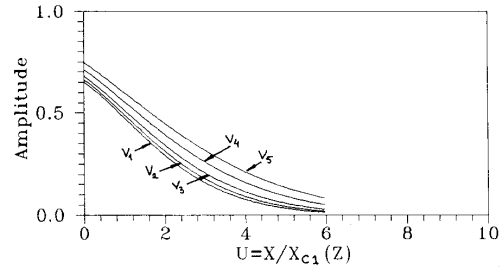


Fig. 9. Mode profiles  $\hat{U}_q$  (for  $q = 1$ ) on the  $v = \text{const.}$  curves of Fig. 7, computed with the corresponding  $\hat{k}_u^2$  distributions in Fig. 8. The calculations near the caustic are performed by the uniform formulation in [1.14, p. 340]. The plot shows  $\hat{U}_q$  as a function of  $u = x/x_{cq}(z)$ .

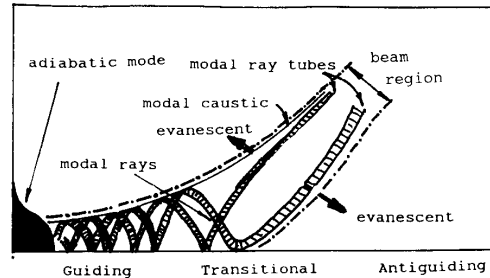


Fig. 10. Qualitative sketch of evolution of modal ray congruences from the well-trapped surface ducted regime to the detached beam in the antiguiding region. After its formation, the second caustic becomes the  $u_1 = \text{const.}$  curve.

propagation in longitudinally and transversely inhomogeneous environments that, in their most general form, can change gradually from being strongly guiding to becoming leaky and eventually antiguiding. An adiabatic mode is an approximate generalization of an exact mode in a coordinate separable guiding environment to environments that are weakly nonseparable; to a lowest order of approximation, the AM adapts smoothly, without cross coupling or reflection, to the changing conditions. The AM cannot describe mode phenomena in cutoff and other transition regions, and they must there be replaced with the more general uniform intrinsic modes. Each IM is synthesized by a continuous spectrum of AM which is generated from the longitudinally dependent

discrete AM eigenvalue by analytic extension. Through this generalization of the AM and IM concepts, an initially well-defined, well-guided mode retains the "modal footprint" even through its transformation into a beam-type wave object via guiding-to-leaky and (or) guiding-to-antiguinding transitions. Source-excited fields in the well-guiding region can be expressed as a superposition of AM or, in transversely open regions, by a hybrid combination of ray and AM fields (see [1.12]). By AM, IM, and ray tracking, these initial fields can then be propagated through the environment.

A major problem in the selection of "best adapted" AM and IM in an environment with relatively arbitrary refractive index variations is the selection of a coordinate frame that renders the wave problem locally separable. This coordinate choice, which parametrizes the problem, is matched to the actual or virtual (caustic) boundaries between which an AM or IM is confined. The study of the canonical problems in [1] and in Section II here has given some insight into the relation between the simplest and most natural original choice of rectangular coordinates and the "correct" curvilinear coordinates that render the problem separable. Based on these observations, a first approximation has here been invoked that reparametrizes the problem from the original rectilinear to a better curvilinear (local circular cylindrical) coordinate frame. When applied to rather general transition problems as in Section III, the curvilinear parametrization, unlike the original rectangular, captures the correct wave phenomenology and therefore comes closer to local separability. Systematic procedures for improvement remain to be developed, but they are expected to rely strongly on the modal ray tracing procedure mentioned in Section III.

The AM and IM, together with the ordinary and generalized (uniformized) ray fields of GTD, provide a combination of wave objects that may be capable of tracking high frequency wavefields over long distances in propagation environments with rather general inhomogeneity profiles. Evidently, the accuracy, efficiency, and ease of computation of such an algorithm remains to be established by numerical experiment, and further refinements of the AM-IM problem are desirable. However, the physical insight gained by tracking these distinct wavefields is bound to help our quantitative understanding of wave propagation phenomena in complex surroundings, and will permit *interpretation* of results obtained purely numerically on large computers.

#### REFERENCES

- [1] L. B. Felsen and L. Sevgi, "Adiabatic and intrinsic modes for wave propagation in guiding environments with longitudinal and transverse variation: Formulation and canonical test," *IEEE Trans. Antennas Propagat.*, pp. 1130-1136, this issue.
- [2] D. Bertilone, A. Ankiewicz, and C. Pask, "Wave propagation in a graded index taper," *Appl. Opt.*, vol. 26, pp. 610-620, 1987.

**Leopold B. Felsen** (S'47-A'53-M'54-SM'55-F'62-LF'90), for a photograph and biography please see page 718 of the July 1985 issue of this TRANSACTIONS.

**Levent Sevgi**, for a photograph and biography please see page 1136 of this issue.